Physics of Fluids

# Advection of droplet collision in centrifugal microfluidics

Cite as: Phys. Fluids **31**, 032003 (2019); https://doi.org/10.1063/1.5082218
Submitted: 20 November 2018 . Accepted: 18 February 2019 . Published Online: 06 March 2019

Xun Liu, Yuan Ji, Yongbo Deng, and Yihui Wu

Physics of Fluids ARTICLE scitation.org/journal/phf

# Advection of droplet collision in centrifugal microfluidics

Cite as: Phys. Fluids 31, 032003 (2019); doi: 10.1063/1.5082218
Submitted: 20 November 2018 • Accepted: 18 February 2019 •
Published Online: 6 March 2019 • Publisher error corrected: 12 March 2019



Xun Liu,[1,2] Yuan Ji,[1,2] Yongbo Deng,[1,2,a)] and Yihui Wu[1,2,b)]

## AFFILIATIONS

[1]State Key Laboratory of Applied Optics, Changchun Institute of Optics, Fine Mechanics and Physics (CIOMP), Chinese Academy of Sciences, Changchun 130033, China
[2]University of Chinese Academy of Sciences, Beijing 100039, China

[a)]Electronic mail: dengyb@ciomp.ac.cn
[b)]Electronic mail: yihuiwu@ciomp.ac.cn

## ABSTRACT

Centrifugal microfluidics has been developed into a powerful technology in chemistry and biology. Its carrier devices allow us to control flows without external pumps, integrate multiple functions onto a disk, and reduce the consumption of reagents or samples. In centrifugal microfluidics, an artificial gravitational field, which determines the volume forces imposed on the microfluid, can be created by the rotating operation of a disc-like microfluidic chip. Centrifugal microfluidics can be a preponderant approach for droplet manipulation because the dimensionless numbers (e.g., the Reynolds number and the Bond number) of the microflows can be controlled by the reasonable design of such a disc-like chip. To study the advection of droplets in a centrifugal microfluidic chip, this paper presents a numerical investigation for the droplet collisions under different Bond numbers and Reynolds numbers. The progress of the collision advection is simulated by solving laminar flow equations and phase-field equations. The distribution of the mixed droplets is described using particle tracking methods. By evaluating the extending ratio of the interface and the barycenter deviation, it is demonstrated that the Bond number and Reynolds number affect different aspects of the advection. For instance, higher Bond numbers produce larger barycenter deviation and higher Reynolds numbers generate a more chaotic distribution. These simulations reveal the advection of droplet collisions under different Bond numbers and Reynolds numbers. Revealing the effects of these dimensionless numbers and advection mechanism can promote more reasonable design and operation of the centrifugal microfluidic platforms.



## I. INTRODUCTION

Centrifugal microfluidic platforms have been extensively developed in recent years. Such platforms have a compact disc-like (CD-like) surface, with all microchannels or chambers fabricated on a disk that is driven to rotate by a motor,[1] which creates an artificial gravity field that applies a volume force to the fluids. The volume force can conveniently be adjusted by tuning the rotating speed and acceleration. Because of this intrinsic driven force, centrifugal microfluidic devices can be designed as closed fluidic systems without any external pumps, which makes it be easy to create multiple complex chambers and channels on one CD-like chip. These advantages have resulted in the realization of many fluidic functionalities, such as the supplying, pre-storage, releasing, and mixing of samples and reagents. Thus, centrifugal microfluidic platforms have been researched in several fields.[2] For instance, centrifugal microfluidics have been applied to nucleic acid analysis and polymerase chain-reaction (PCR) studies, the separation of cells or particles that can only be realized by a centrifugal field or assembling some other external field,[3–6] and environmental analyses.

Droplet-based microfluidic platforms use droplets to bring about reactions between samples and reagents. They offer significant advantages in fabricating special materials and chemical products,[7,8] can reduce the consumption of samples, and enable simple repetitions of concurrent tests. Droplet-based microfluidics often requires several external pumps and transports droplets at low velocity. This results in the challenges on mixing two droplets. With the help of a centrifugal platform, the droplets can be driven at high velocity by the volume force, whereby the droplet collision occurs at the expected velocity and produces better mixing performance.

The impact velocity can directly affect the initial kinetic energy in collision, and the rotational speed can control the centrifugal acceleration which determine the volume force and affect the pressure in the collision.

Droplet collision can be considered as a multiphase problem.[9–11] Centrifugal microfluidic systems have the physical progress of a liquid phase replacing the gaseous phase. To investigate the advection mechanism of droplet collisions, the diffuse-interface method, which is popular in solving multiphase problems, can be used to capture the dynamic interface between the air and the droplets.[12,13] In the mixed droplets, particle tracking methods can be used to analyze the mixing distributions[14] and to investigate the mixing performance of the droplet-collision. Several mixing evaluation methods and indexes have been reported.[15,16] These existing methods can reflect the mixing performance in some respects, but not all of them can precisely evaluate the performance of the mixing processes. In droplet collisions, better mixing performance corresponds to a more chaotic distribution or longer interface between the two droplet-components. Evaluation of the interface between the mixed droplets is more applicable to advection of droplet-collision. Moreover, in the mixing process of two droplets, the barycenters of each droplet approach that of the mixed droplet. The distance between the barycenter of the original droplets to that of the final mixed droplet reflects the location change of the droplets in the collision process. In centrifugal microfluidic platforms, the volume forces, which can be considered as an artificial gravity on the droplet, are affected by the rotating speed and disk radius. These parameters can be characterized by the Bond number, a dimensionless parameter of fluid mechanics. Because different collision conditions produce different distributions, this enables to form special droplets or achieve better mixing performance.

The collisions of droplets can be investigated by dimensionless numbers from different viewpoints. The Weber number, the ratio of the inertial forces to the surface tension, is the widely used parameter in the research of droplets collision, such as the maximum spreading of a droplet impact the solid surface[17] and viscous energy dissipation in droplet-droplet collision.[18] The Reynolds number, the ratio of the inertial forces to viscous forces, often performs the similar role as the Weber number in droplets collision.[19,20] Other dimensionless numbers like the capillary number, the ratio of viscous forces, and surface tension can also characterize the collision evolution of two droplets;[18] and the Ohnesorge number, the ratio of the viscous forces to the surface tension and inertial forces, can dimensionally describe the droplet deformation.[21] Other parameters like the droplets size, the contact angle, and even the temperature can all make the collision evolve differently.[22] The Reynolds number can also be calculated according to the Weber number and the capillary number[18] or Ohnesorge number[20] because the capillary number is the ratio of the Weber number to the Reynolds number. In this paper, the mixing of two droplets is implemented by a moving droplet colliding a static one, where both the Reynolds number and the Weber number can be used characterize the relative importance of inertial forces. Then, the effect of the Reynolds number has been mainly investigated for the droplet collision.

In the following, we present a phase-field model of two-phase flow for droplet collisions in a microchannel. The mixing performance is evaluated using the mixing interface length extension rate, and the results of droplet collisions are appraised by examining the barycenters. To study the advection induced by the droplet collisions, the effects of the dimensionless Reynolds and Bond numbers on the distribution and mixing quality of the droplets are investigated.

## II. METHODOLOGY

The methods for modeling and evaluating the advection of droplet collision in centrifugal microfluidics are presented as follows.

### A. Theoretical model

The fluid flow of the droplet motion, which moves as a slug in a channel, is described using the diffuse-interface method. In the diffuse-interface method, the singularity at the contact line of the two-phase flow is regularized by the Cahn–Hilliard diffusion, and the essential no-slip condition is imposed on the wall boundary. The liquid slug motion in the centrifugal platform is governed by the coupling system of the Navier–Stokes equations and the Cahn–Hilliard equations,

$$\begin{aligned} \rho\left(\frac{\partial \mathbf{u}}{\partial t}+\mathbf{u}\cdot\nabla\mathbf{u}\right) &= \nabla\cdot\left[-p\mathbb{I}+\mu\left(\nabla\mathbf{u}+\nabla\mathbf{u}^{\mathrm{T}}\right)\right]+\psi\nabla\phi+\mathbf{f},\\ -\nabla\cdot\mathbf{u} &= 0,\\ \frac{\partial\phi}{\partial t}+\mathbf{u}\cdot\nabla\phi &= \nabla\cdot(M\nabla\psi),\\ \psi &= -\nabla\cdot(\lambda\nabla\phi)+\frac{\lambda}{\epsilon^2}\phi\left(\phi^2-1\right), \end{aligned} \tag{1}$$

where $t$ denotes time; $\rho$ is the fluid density; $\mu$ is the dynamic viscosity of the fluid; $\mathbf{u}$ is the fluid velocity; $p$ is the pressure; $\mathbb{I}$ is the unitary tensor; $\lambda$ is the mixing energy density, determined according to the relation between the mixing energy density and surface tension $\sigma=\frac{2\sqrt{2}}{3}\frac{\lambda}{\epsilon}$; $\varepsilon$ is the capillary width, chosen based on the element size; $M$ is the mobility or Onsager coefficient; $\phi$ is the phase-field variable, with $\phi=\pm1$ in the two bulk phases and $\phi=0$ on the two-phase interface; $\psi$ is the chemical potential; $\psi\nabla\phi$ is the capillary force;[23] and $\mathbf{f}$ is the volume force loaded on the fluid, which includes the centrifugal force $-\rho\boldsymbol{\omega}\times(\boldsymbol{\omega}\times\mathbf{r})$, Coriolis force $-2\rho\boldsymbol{\omega}\times\mathbf{u}$, and Euler force $-\rho\frac{\mathrm{d}\boldsymbol{\omega}}{\mathrm{d}t}\times\mathbf{r}$ in the centrifugal platform.[24] The density and dynamic viscosity are functions of the phase-field variable,[25]

$$\begin{aligned} \rho &= \rho_1\frac{1-\phi}{2}+\rho_2\frac{1+\phi}{2},\\ \mu &= \mu_1\frac{1-\phi}{2}+\mu_2\frac{1+\phi}{2}, \end{aligned} \tag{2}$$

where $\rho_1$ and $\rho_2$ are the densities of the two fluids, respectively; $\mu_1$ and $\mu_2$ are the dynamic viscosities of the two fluids, respectively. The boundary conditions of the coupled system are set as follows:

- Initial condition:

$$\begin{aligned} \mathbf{u}|_{t=0} &= \mathbf{u}_0,\\ \phi|_{t=0} &= \phi_0, \end{aligned} \tag{3}$$

- Initial interface:

$$\phi_0 = 0, \tag{4}$$

- Boundary condition at the inlet:

$$\left[-p\mathbb{I}+\mu\left(\nabla\mathbf{u}+\nabla\mathbf{u}^{\mathrm{T}}\right)\right]\cdot\mathbf{n}=\mathbf{0},$$
$$\mathbf{n}\cdot(M\nabla\psi)=0, \tag{5}$$
$$\phi=-1,$$

- Boundary condition at the wall:

$$\mathbf{u}=\mathbf{0},$$
$$\mathbf{n}\cdot(M\nabla\psi)=0, \tag{6}$$
$$\mathbf{n}\cdot(\lambda\nabla\phi)=0,$$

- Boundary condition at the outlet:

$$\left[-p\mathbb{I}+\mu\left(\nabla\mathbf{u}+\nabla\mathbf{u}^{\mathrm{T}}\right)\right]\cdot\mathbf{n}=\mathbf{0},$$
$$\mathbf{n}\cdot(M\nabla\psi)=0, \tag{7}$$
$$\mathbf{n}\cdot(\lambda\nabla\phi)=0,$$

where $\mathbf{u}_0$ and $\phi_0$ are the initial velocity and phase variable, respectively. In the finite-element solution of the coupled system in Eq. (1), triangular elements are used for the Navier–Stokes equations and Cahn–Hilliard equations, where the fluid velocity and pressure are interpolated quadratically and linearly,[26] respectively. The phase-field variable and chemical potential are both interpolated quadratically. Numerical simulations of the collision of liquid slugs in a centrifugal platform are performed using the commercial finite element software *COMSOL Multiphysics*,[27–30] where the simulation parameters are set as listed in Table I.

## B. Lagrangian description of collided droplets

To investigate the distribution of the two droplet components after collision, a particle-tracking method is used in the numerical simulation. The particle-tracking method uses a massless particle group to represent each liquid droplet, and this makes the advection of these particles, collision process, and mixing phenomena be visualized.[9,31] These particles neither interact with each other nor exhibit diffusion via random motion; they flow along streamlines. The trajectories of the particles are computed using the Lagrangian method, which records the spatial positions of the particles at each time step. The particle advection equations are defined as[32]

$$\frac{\mathrm{d}\mathbf{x}}{\mathrm{d}t}=\mathbf{u}, \tag{8}$$

**TABLE I**. Parameters used to simulate droplet collisions in a centrifugal microfluidic platform.

| $\rho_1$ (kg/m$^3$) | $\rho_2$ (kg/m$^3$) | $\mu_1$ (Pa s) | $\mu_2$ (Pa s) | $\varepsilon$ (m) | $M$ (m$^2$ s/kg) |
|---|---|---|---|---|---|
| $1\times10^3$ | 1 X $10^0$ | $1\times10^{-3}$ | $1\times10^{-5}$ | $10^{-5}$ | 50 |

where $x$ is the particle position vector. The fourth-order Runge–Kutta method with an adaptive step size is used to integrate Eq. (8) numerically. Finally, the distribution of the particles is computed. All particle positions can be determined using the solution of the phase-field model. The used particle-tracking method is the forward type. In such particle-tracking process, some particles are stopped on the walls and the distortion of the particle group causes the non-uniform distribution of the particles. These result in the related tolerance. And such tolerance is decreased by reasonably increasing the number of particles in this paper.

In the two-phase flow, the particles representing the two droplets being mixed move with the droplets, so they reflect the motion and certain phenomena of the droplet collision process. When there is enough number of points on the trajectories, the distribution of the particles can approximate the distribution of the droplets. If we define an indicator value for the particles from different droplets, then the mixed droplet in the same phase can be divided into two different particle groups based on the indicator values. By defining the different particle groups with the indicator values $p=+1$ or $p=-1$, the distribution of original droplets in the mixed droplet can be determined. Moreover, interpolating between positions and identity values for all particles, the contour line $p=0$ gives the interface between the original droplets.

## C. Evaluation of advection

Unlike the mixing quality evaluation based on tracer statistics[33] or the liquid concentration,[34] we evaluate the mixing based on the whole distribution. And two evaluation methods are used: the interface extension rate and the deviation of barycenters.

When one droplet impacts another, the droplets will advect and diffuse. All the motion of the droplets, such as stretching, collision, rotation, and disjunction, improves the mixing performance and helps to extend the interface. In Fig. 1(a), the two colors indicate the different original droplets before the mixing process. From the interface between the two original droplets, it can be confirmed that the interface length can be used to evaluate the advection and mixing performance, where a longer interface indicates stronger advection and better mixing. To make the index more rational, we define the mixing interface extension rate which uses the length ratio of the final mixed interface to the unmixed interface as one of the evaluating index of mixing. The unmixed interface is demonstrated in

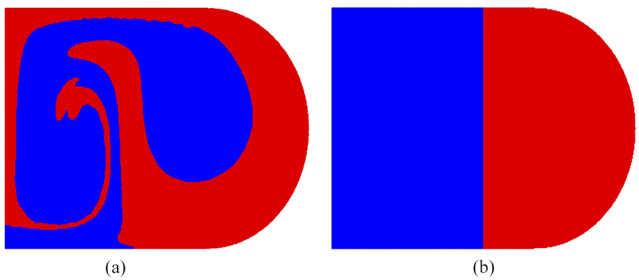


**FIG. 1**. Distributions of mixed droplet and unmixed droplet. (a) is the mixed droplet, the different colors denote the original droplets in the mixed droplet. (b) is the situation of two neighboring droplets without mixing.

Fig. 1(b), and its length is the characteristic length, which is defined to be the width of the microchannel.

Another index for evaluating the distribution is the deviation of barycenters, which is the barycenter distance difference between the mixed droplets and the original ones. The two original droplets have the same density; hence, the barycenters can be calculated by averaging the coordinates of the particle group used in the particle-tracking method. The deviation of barycenters can reflect the liquid distribution of the original moving droplet as a component of the mixed one, where smaller derivation between the barycenter of the original moving component and that of the mixed droplet corresponds to better mixing performance.

## III. RESULTS AND DISCUSSION

The schematic of the simulation geometry is shown in Fig. 2. The microfluidic structures in a test-tube shape lies on a rotating chip along the radial direction, and all fluidics are driven by the volume force caused by the centrifugal operation. Such choice of the geometry is because of the wide existence of the microfluidic structure formed by a microchamber connected with two microchannels on a CD-like microfluidic chip, where the two microchannels are, respectively, used to transport liquid to the chamber and connect a vent hole.[1] The simulations are conducted for different values of the Reynolds number. By assigning different initial velocity $u_0$ which ranges from 0 to 3.2 m/s, the Reynolds number can be varied. The Reynolds number of collision is calculated based on the velocity of droplet A at the time step before collision. This is because droplet A will accelerate for a short distance before collision. Simulations were conducted with different values of the Reynolds number *Re* and the Bond number *Bo* to investigate the advection of droplet collision in centrifugal microfluidics. Figure 3 shows the general process of the collision and mixing corresponding to $Bo = 0.5778$ and $Re = 159.74$; and Fig. 4 shows the evolution of the maximal velocity in the process. The angular velocity is set to be 3000 rad/min. During the rotation, one droplet is accelerated by the centrifugal force; furthermore, Coriolis force is generated and imposed. Based on the common action of centrifugal and Coriolis forces, the droplet A starts moving to collide. This collision process contains several steps. First, droplet A moves toward droplet B at one side with an initial velocity, resulting in a collision; then, the impact forms a resilient mixed droplet, which moves in the opposite direction to the centrifugal force for a short distance before the finally static status.

To investigate the effect of the Bond number, the Reynolds number in the collision kept to be invariant. In the schematic shown in Fig. 5, the collision occurs with an accelerated droplet A. To ensure the constant Reynolds number, the geometry is constructed based on the shapes of the droplets at the time step before collision. Because large *Re* can make the droplet shape be quite unstable, its initial value should not be too large. By assigning a different rotation speed or centrifugal radius, different Bond numbers can be produced. In the simulations, the Mach number is less than 0.3. Therefore, the compression effect of air flow is negligible.

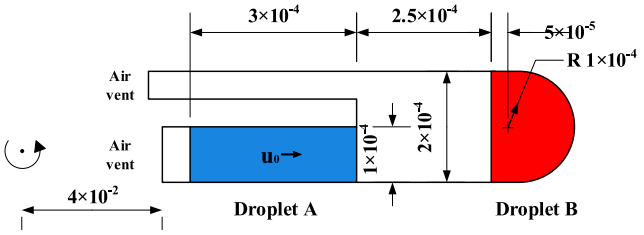


**FIG. 2**. Schematic of the simulation geometry for various Reynolds numbers and fixed Bond number, where the droplet A and droplet B are in the theoretical static state with sharp edges at rest. (Unit in the graph is m.)

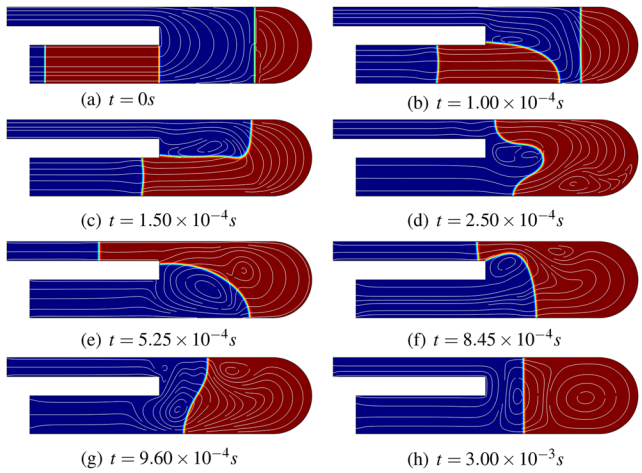


**FIG. 3**. Collision process of the droplets in a centrifugal microfluidic platform. At $t = 0$, droplet A starts to move toward droplet B with an initial velocity $u_0 = 2$ m/s; then, a collision occurs and droplet A presses into droplet B, causing the resilient part to move in the opposite direction to the centrifugal force; furthermore, the resilient part makes bounce-back motion, which results in the wobble liquid/air interface; ultimately, the liquid interface calms down to its stable status.

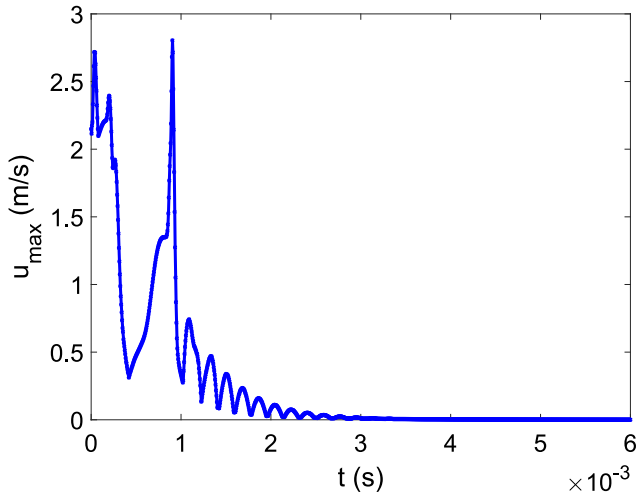


**FIG. 4**. Evolution of maximal velocity in the collision process. The maximal velocity tends to be 0 after $3.00 \times 10^{-3}$ s which means the droplets calms down to a stable status with the least potential energy.

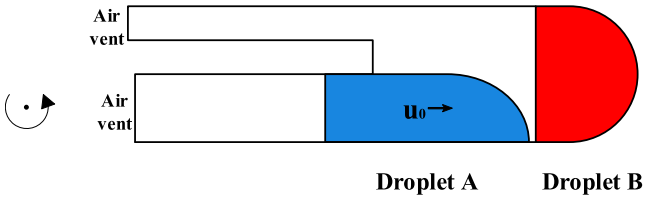


**FIG. 5**. Schematic of the simulation geometry for different Bond numbers and the same Reynolds number based on the shape of droplets at the time step before collision in the previous simulation with a fixed Bond number.

### A. Effect of Reynolds number

The Reynolds number of the impact droplet is calculated based on the velocity at the time step before collision. The Reynolds number is calculated as

$$Re = \frac{\rho u L}{\mu}, \tag{9}$$

where $\rho$ is the density and $u$ is defined to be the average velocity of the droplet; $L$ is the characteristic size of the droplet; in this case, the droplet in the microchannel moves as a slug. Instead of using the droplet diameter in calculating the Reynolds number,[18] the characteristic size is set as the width of the slug, which is the same as the characteristic length of the microchannel.

The Reynolds number *Re* has notable influence on the droplet motion. In the microchannel, the droplet velocity close to the wall is smaller than in the center, which means the center of the droplet has a larger displacement than the margin fluid. Figure 6 shows the moving-droplet shapes corresponding to different Reynolds numbers. When *Re* is 170, it is the deformation of the droplet is unconspicuous. However, as *Re* increases, the droplet has a forward bulge at the front and a concavity at the rear. The bulge changes slightly at higher *Re*, while the concavity becomes much deeper as *Re* increases from 530 to 850, and the droplet becomes extended at high *Re*. At very high *Re*, the droplet will become unstable and will burst from the concave bottom.

To avoid bursting and large deformations, *Re* is not set too large in the collision simulations. As shown in Fig. 7, the Reynolds numbers of the two conditions are very similar, but the distributions are quite different. In the collision process, a resilient part is formed, and this moves into the air vent before the final calming down. If the Reynolds number were too large, the rebound part may separate

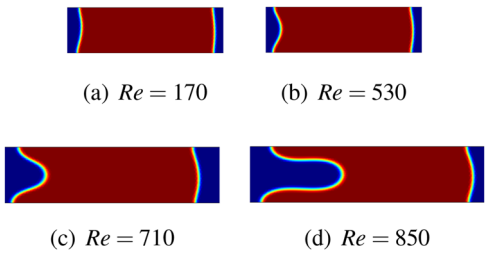


**FIG. 6**. Shape of moving droplet in channel at different *Re*. In the channel, the velocity near the wall is slower than in the center. This difference is enhanced at higher *Re*.

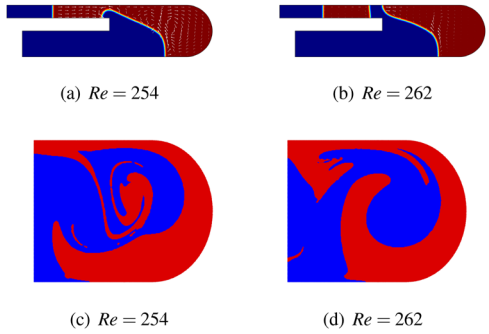


**FIG. 7**. Similar *Re* values before the first collision cause two totally different distributions corresponding to *Bo* = 1.6050. *Re* = 254 in (a) and (c), whereas *Re* = 262 in (b) and (d). (a) and (b) show the rebound part of the mixed droplet after collision. (c) and (d) show the final distribution of the two droplets after their collision.

from the mixed droplet, and the separated part would finally drop and cause another collision. This would make the distribution quite different. Thus, the Reynolds number is set to be less than the value that causes this separated resilient part.

As *Re* is low enough to avoid the second collision, the distribution shown in Fig. 8 can be obtained. Corresponding to *Re* = 62.97, droplet B surrounds droplet A with a simple interface. As *Re* increases, droplet A extends within the mixed droplet. Corresponding to *Re* larger than 159.74, droplet A extends two branches and rolls. Corresponding to *Re* = 240.22, the interface becomes rougher than the case of *Re* = 224.54. The distribution is more chaotic at larger values of the Reynolds number.

The maximal pressure in the collision process is shown in Fig. 9, where the maximal pressure increases rapidly at the start and then quickly drops in the collision progress. The maximum pressure is higher corresponding to larger *Re*, which indicates that large *Re* is related to high-pressure collisions. After the collision, the maximal pressure reaches a constant value. *Bo* is fixed in this simulation, and the final maximal pressures are independent of *Re*, where the pressure value is taken at the maximal radial position of the microchannel.

In terms of the evaluation index, Fig. 10 shows the interface extension rate. From Fig. 10, it can be concluded that increase *Re* is helpful for extending the interface, with an extension factor of 3.214 at *Re* = 62.79 raising to 5.31 at *Re* = 261.16. These values show that larger *Re* makes the mixing action (i.e., moving and rotating) more acute, and these motions stir the droplets and stretch the interface.

The second index, the deviation of barycenters, is shown in Fig. 11. Because of the geometry of the microchannel, the deviation of barycenters in the $x$ direction (radial direction) is actually lager than the deviation in the $y$ direction (circumferential direction). The deviation in the $y$ direction, $d_y$, increases slightly when *Re* is larger than 120, but is quite small compared with the deviation in the $x$ direction. The deviation distance $d$ and the deviation in the $x$ direction, $d_x$, do not exhibit any change when *Re* is smaller than 120, but as *Re* increases, $d_x$ decreases to almost half the value at *Re* = 63. For larger Reynolds numbers, the barycenters of the original droplets are close to the barycenter of the whole mixed droplet, meaning that the distribution at high *Re* is more balanced. Similar to the extension

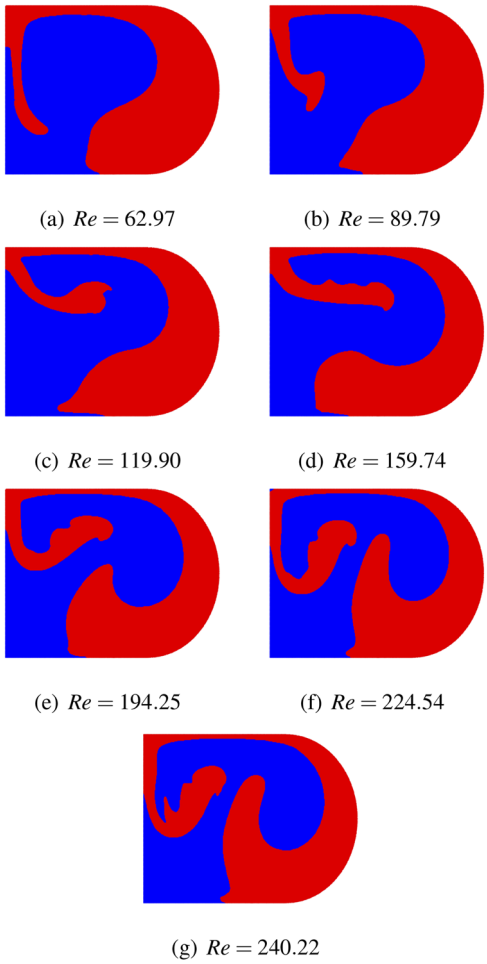


**FIG. 8**. Distributions of droplets at different *Re* and fixed *Bo* = 0.5778. As the droplet moves in the mixing tube with a velocity of 0, *Re* increases to 62.97 before the collision. When *Re* is less than 240.22, the droplet will not separate after the first collision.

rate, a larger Reynolds number can improve the mixing performance during the droplet collision process.

When *Re* is too large, droplet A may burst before collision, which may even affect droplet B. In Fig. 12, the deep concavity causes the droplet to burst, resulting in a new collision. Furthermore, this separated part may directly move into the vent channel if its mass is low enough. Moreover, speedy droplets can press the air, deforming droplet B. In this situation, the final distributions are very complicated and it is difficult to determine whether the large *Re* or the burst droplet affect the collision more significantly.

The Reynolds number can directly affect the distribution, with larger *Re* leading to more chaotic and balanced distributions while making the interface rougher. Larger values of *Re* can even make the collision process more complicated.

### B. Effect of Bond number

The Bond number is a dimensionless parameter reflecting gravitational forces and surface tension. In the centrifugal platform, the

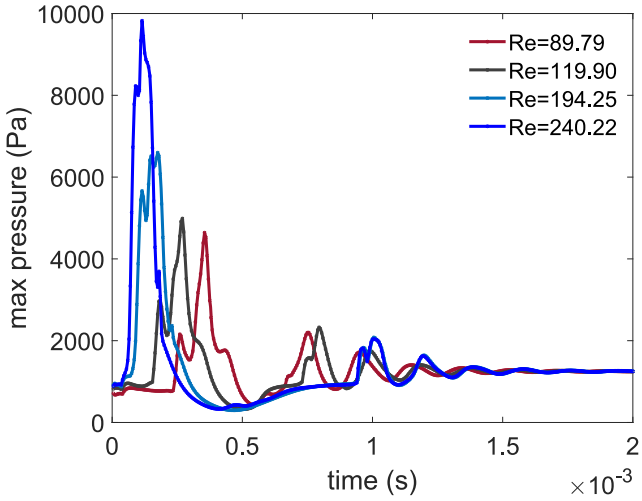


**FIG. 9**. Maximal pressure in the mixing process for a fixed *Bo*. Lager *Re* corresponds to larger velocity, which makes the collision occur earlier. The maximal pressure is prone to be around the bottom of the mixing chamber which has the maximal rotating radius; however, the position of maximal pressure is changing in the collision process.

centrifugal forces can be considered as artificial gravitational forces acting on the flow. The Bond number in the centrifugal microfluidic platform can be calculated as

$$Bo = \frac{\Delta\rho\omega^2 RL^2}{\sigma}, \tag{10}$$

where $\Delta\rho$ is the density difference of liquid and gaseous phases; $\omega$ is the rotational speed of the centrifugal platform; $R$ is the radius of gyration of one point; $L$ is the characteristic length (the characteristic length of a droplet is its radius); and $\sigma$ is the surface tension. In attempting to fix *Re* while varying *Bo*, it is challenging to control the

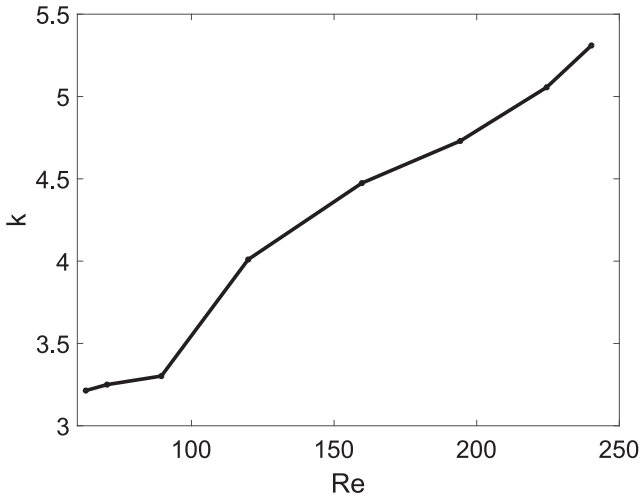


**FIG. 10**. Extension rate of the interface between the original droplets in the mixed droplet for different *Re*.

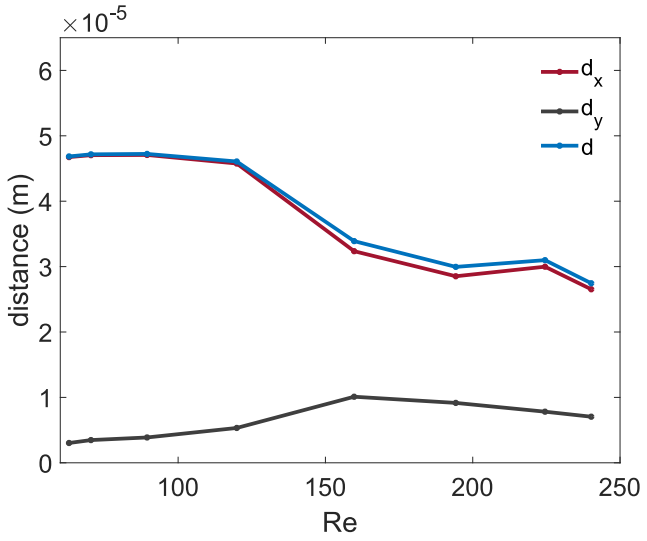


**FIG. 11**. Deviation of barycenters: average distance between the original droplets' barycenters and the mixed droplet barycenter for different *Re*.

velocity in the centrifugal platform. To keep the *Re* to be invariant, droplet A must be positioned near to droplet B with a low velocity because the droplet shape is barely affected at low *Re*.

The distributions at different values of *Bo* with a fixed *Re* are quite different, as shown in Fig. 13. These distributions may appear similar but have different details. In the distributions, it can deduce that droplet A hits droplet B and rolls. A small part of the droplet B rolls into the center of the mixed droplet, and this small part maintains contact with the original droplet through a long tail. The tail becomes slenderer and exhibits more acute rotation as *Bo* increases. For such observation, because the pressure of the static droplet is high in the condition of large Bond number, fluid diffusion is not

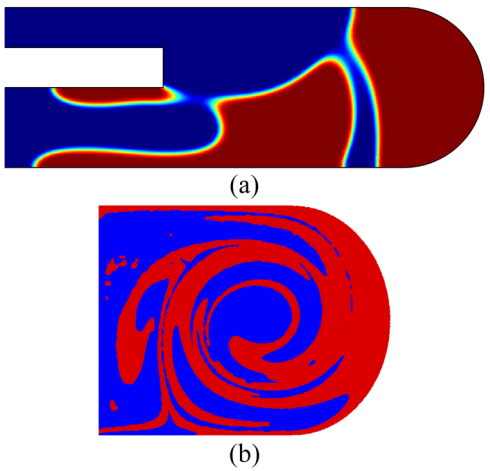


**FIG. 12**. (a) In this situation, *Re* is greater than 800 and *Bo* = 3.515. The distorted droplet bursts into serval pieces when it moves into the wider channel. (b) Distribution of original droplets in the mixed droplet.

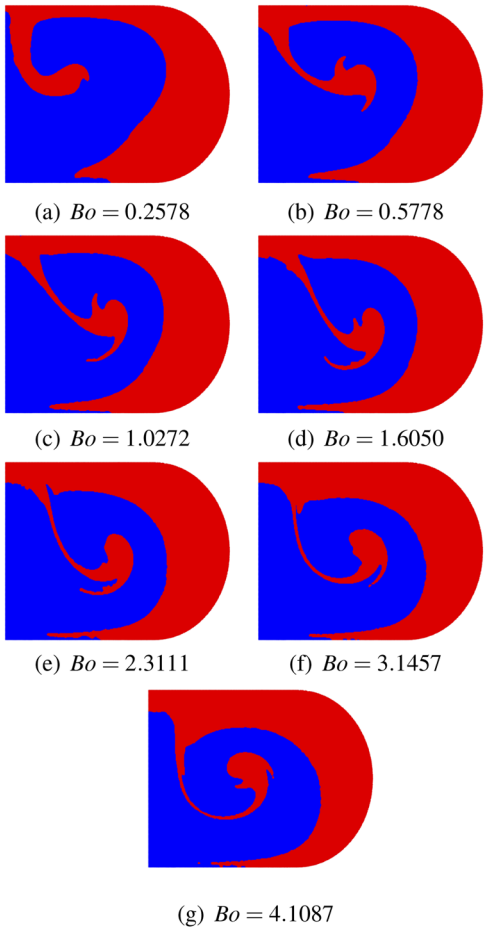


**FIG. 13**. Distributions of droplets at different *Bo* for fixed *Re* = 150.

efficient and the velocity of droplet decrease quickly. However, to release the kinetic energy, the droplet moves toward the low pressure region which is around the original position of the moving droplet.

In centrifugal microfluidics, a larger value of *Bo* corresponds to larger artificial gravity and stronger external force. According to the Navier–Stokes equation, stronger external force produces higher pressure, which is shown in Eq. (1). As shown in Fig. 14, the first peaks of the maximal pressure indicate the collision. At larger values of the Bond number, the pressure in the collision is higher. Moreover, the maximal pressure at larger Bond numbers remains higher throughout the collision and mixing process in the same time step. The higher pressure means that the liquid is less likely to diffuse.

Figure 15 shows the interface extension rate at different values of *Bo*. There is little difference in the interface extension rate. When *Bo* is less than 0.5778 or greater than 1.0272, the interface extension rates do not change, as shown in Fig. 13. However, for *Bo* in the range 0.5778–1.0272, the index raises and the distribution becomes more complicated. The changes in the extension rate are caused by the long tail in the rolled part of the droplet.

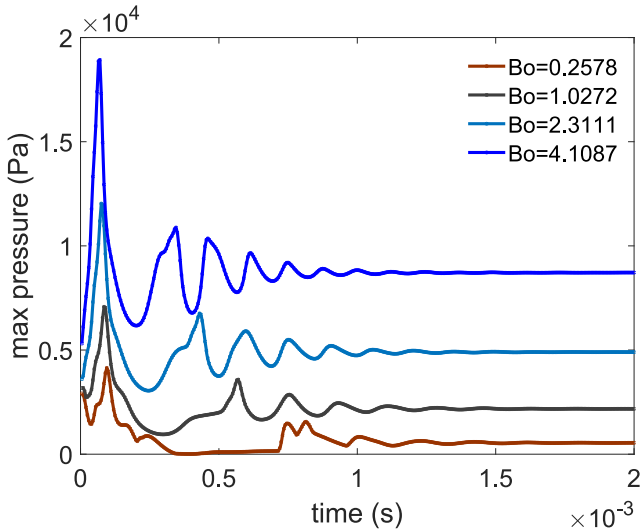


**FIG. 14**. Maximal pressure in the mixing process for a fixed *Re* = 150.

The deviation in the barycenters in Fig. 16 shows a clear tendency with respect to *Bo*. The deviation in the *y* direction, $d_y$, is larger under high Bond numbers, increasing by a factor of almost ten, from *Bo* = 0.5778 to *Bo* = 4.1087. The deviation in the *x* direction, $d_x$, decreases as *Bo* increases. As a result, the general barycenter deviation *d* remains almost constant. This is because that a larger Bond number corresponds to larger artificial gravitational acceleration and a larger volume force, which creates higher pressure according to Eq. (8). This higher pressure restrains the movement in the *y* direction, forcing droplet A to move in the *x* direction.

Based on the above results, the Bond number does not affect the collision directly, but larger Bond numbers make it more difficult for the droplet to move. As one droplet impacts another in the *x* direction, the larger Bond number makes it be difficult for the droplet to move and diffuse in the *y* direction. Thus, the moving droplet has to roll to release its kinetic energy, which makes the tail longer and produces more acute rotation.

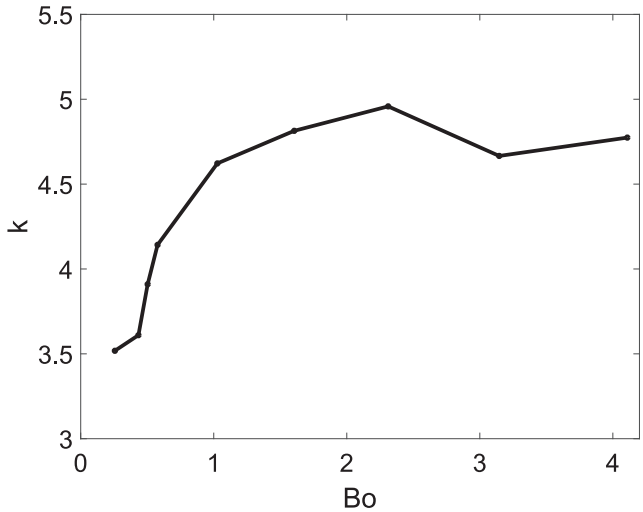


**FIG. 15**. Extension rate of the interface between the original droplets and the mixed droplet for different *Bo*.

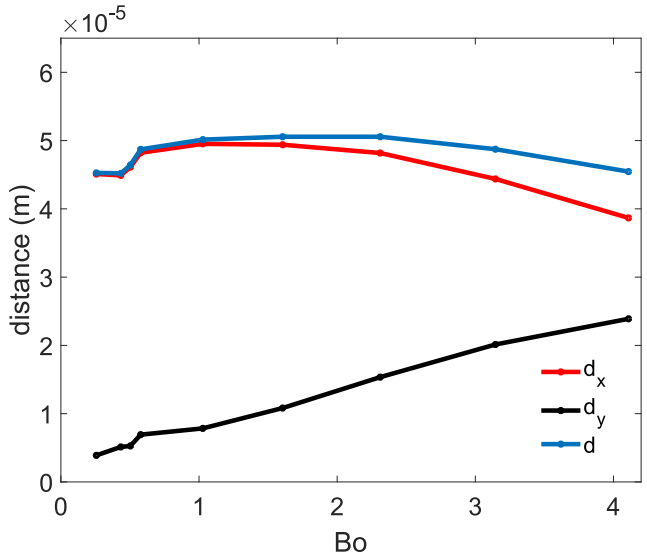


**FIG. 16**. Deviation of barycenters: average distance between the original droplets' barycenters and the mixed droplet barycenter for different *Bo*.

## IV. CONCLUSIONS

We have described a model for droplet collision in centrifugal microfluidics and studied the distribution of the original droplets in the mixed droplet after collision under various conditions. The Reynolds number and Bond number were set by controlling the rotational speed and the velocity of collision. The interface extension rate and the deviation of barycenters were used to evaluate the strength of advection and mixing performance. The simulation results show that large Reynolds numbers can cause powerful collisions and unstable droplets, leading to chaotic distributions. As shown in this paper, the interface extension rate and the deviation of barycenters exhibit obvious changes when *Re* is larger than 120. This indicates that larger *Re* is related to a longer mixing interface and more uniform distribution, which signifies better mixing performance. Larger values of *Bo* make diffusion be more difficult, but can produce more rotation, which stretches the mixing interface. When *Bo* is approximately 1, the interface extension rate reaches a maximum and the deviation of barycenters approaches a minimum. In summary, to produce an even distribution or better mixing performance, the system should have higher *Re* to ensure a violent collision. Choosing a suitable *Bo* aids diffusion and produces a longer mixing interface. Suitable values of the Reynolds number and Bond number can help centrifugal microfluidic systems to attain their expected performance. This current research mainly focuses on two dimensional case, and the volume effects and experimental investigations will be further implemented in the future.

## ACKNOWLEDGMENTS

This work was supported by the National Natural Science Foundation of China (Nos. 51875545 and 61727813), the Youth Innovation Promotion Association of the Chinese Academy of Sciences (No. 2018253), and the Open Fund of SKLAO.

## REFERENCES

[1]O. Strohmeier *et al.*, "Centrifugal microfluidic platforms: Advanced unit operations and applications," Chem. Soc. Rev. **44**(17), 6187 (2015).
[2]M. Tang *et al.*, "A review of biomedical centrifugal microfluidic platforms," Micromachines **7**(2), 26 (2016).
[3]R. Burger *et al.*, "Centrifugal microfluidics for cell analysis," Curr. Opin. Chem. Biol. **16**(3-4), 409 (2012).
[4]T. Morijiri *et al.*, "Sedimentation pinched-flow fractionation for size- and density-based particle sorting in microchannels," Microfluid. Nanofluid. **11**(1), 105 (2011).
[5]T. Morijiri *et al.*, "Microfluidic counterflow centrifugal elutriation system for sedimentation-based cell separation," Microfluid. Nanofluid. **14**(6), 1049 (2013).
[6]P. Sajeesh and A. K. Sen, "Particle separation and sorting in microfluidic devices: A review," Microfluid. Nanofluid. **17**(1), 1 (2014).
[7]R. Seemann *et al.*, "Droplet based microfluidics," Rep. Prog. Phys. **75**(1), 016601 (2012).
[8]S. Mashaghi *et al.*, "Droplet microfluidics: A tool for biology, chemistry and nanotechnology," Trends Anal. Chem. **82**, 118 (2016).
[9]K. Sun *et al.*, "Collision-induced jet-like mixing for droplets of unequal-sizes," Int. J. Heat Mass Transfer **120**, 218 (2018).
[10]H. Gu *et al.*, "Droplets formation and merging in two-phase flow microfluidics," Int. J. Mol. Sci. **12**(4), 2572 (2011).
[11]Z. Xu *et al.*, "Numerical simulation on fluid mixing by effects of geometry in staggered oriented ridges micromixers," Sens. Actuators, B **153**(1), 284 (2010).
[12]C. Liu and J. Shen, "A phase field model for the mixture of two incompressible fluids and its approximation by a Fourier-spectral method," Physica D **179**(3), 211 (2003).
[13]P. Yue *et al.*, "A diffuse-interface method for simulating two-phase flows of complex fluids," J. Fluid Mech. **515**, 293 (2004).
[14]P. Garg *et al.*, "Chaotic mixing in a planar, curved channel using periodic slip," Phys. Fluids **27**(3), 032004, (2015).
[15]T. G. Kang and T. H. Kwon, "Colored particle tracking method for mixing analysis of chaotic micromixers," J. Micromech. Microeng. **14**(7), 891 (2004).
[16]M. Camesasca *et al.*, "Entropic characterization of mixing in microchannels," J. Micromech. Microeng. **15**(11), 2038 (2005).
[17]H. Huang *et al.*, "Energetic analysis of drop's maximum spreading on solid surface with low impact speed," Phys. Fluids **30**(2), 022106 (2018).
[18]G. Finotello *et al.*, "Effect of viscosity on droplet-droplet collisional interaction," Phys. Fluids **29**(6), 067102 (2017).
[19]M. Ebrahim *et al.*, "Simulation of the spreading of a gas-propelled micro-droplet upon impact on a dry surface using a lattice-Boltzmann approach," Phys. Fluids **29**(7), 072104 (2017).
[20]G. Charalampous *et al.*, "Collisions of droplets on spherical particles," Phys. Fluids **29**(10), 103305 (2017).
[21]Z. Zhang *et al.*, "Kinetic energy recovery and interface hysteresis of bouncing droplets after inelastic head-on collision," Phys. Fluids **29**(10), 103306 (2017).
[22]S. A. Banitabaei *et al.*, "Droplet impact onto a solid sphere: Effect of wettability and impact velocity," Phys. Fluids **29**(6), 062111 (2017).
[23]P. Yue *et al.*, "Phase-field simulations of interfacial dynamics in viscoelastic fluids using finite elements with adaptive meshing," J. Comput. Phys. **219**(1), 47 (2006).
[24]Y. Deng *et al.*, "Euler force actuation mechanism for siphon valving in compact disk-like microfluidic chips," Biomicrofluidics **8**(2), 024101 (2014).
[25]M. R. Rokhforouz *et al.*, "Phase-field simulation of counter-current spontaneous imbibition in a fractured heterogeneous porous medium," Phys. Fluids **29**(6), 062104 (2017).
[26]H. C. Elman *et al.*, "Finite elements and fast iterative solvers: With applications in incompressible fluid dynamics," *Numerical Mathematics and Scientific Computation* (Oxford University Press, 2014).
[27]See http://www.comsol.com for software information about COMSOL Multiphysics.
[28]See https://www.comsol.com/model/capillary-filling-8212-phase-field-method-1878 for phase-field modelling information in COMSOL Multiphysics.
[29]D. Conchouso *et al.*, "Simulation of a 3D flow-focusing capillary-based droplet generator," in Proceedings of the COMSOL Conference, Rotterdam, 2013.
[30]I. I. Bogdanov *et al.*, "Direct pore-scale modeling of two-phase flow through natural media," in Proceedings of the COMSOL Conference, Stuttgart, 2011.
[31]R. S. R. Sidin *et al.*, "A Lagrangian approach to droplet condensation in atmospheric clouds," Phys. Fluids **21**(10), 106603 (2009).
[32]P. S. Contreras *et al.*, "Topological analysis of a mixing flow generated by natural convection," Phys. Fluids **28**(1), 013602 (2016).
[33]J. V. Karaeva and G. R. Khalitova, "Evaluation of mixing quality in anaerobic digester," J. Renewable Sustainable Energy **7**(5), 053111 (2015).
[34]G. Kabacaoglu *et al.*, "Quantifying mixing in vesicle suspensions using numerical simulations in two dimensions," Phys. Fluids **29**(2), 021901 (2017).